Published in final edited form as:
Bone. 2012 September ; 51(3): 535–545. doi:10.1016/j.bone.2012.05.008.

Vascular Development during Distraction Osteogenesis Proceeds by Sequential Intramuscular Arteriogenesis Followed by Intraosteal Angiogenesis

Elise F. Morgan, Ph.D.[1,3], **Amira I. Hussein, M.S.**[1], **Bader A. Al-Awadhi, D.D.S.**[2], **Daniel E. Hogan, M.A.**[1], **Hidenori Matsubara, M.D.**[3], **Zainab Al-Alq, D.D.S.**[4], **Jennifer Fitch, Ph.D.**[3], **Billy Andre, B.S.**[1], **Krutika Hosur**[1], and **Louis C. Gerstenfeld, Ph.D.**[3]

[1]Orthopaedic and Developmental Biomechanics Laboratory, Department of Mechanical Engineering, Boston University, Boston, MA 02215

[2]Department of Prosthodontics, Boston University School of Dental Medicine, Boston, MA 02118

[3]Orthopaedic Research Laboratory, Department of Orthopedic Surgery, Boston University School of Medicine, Boston, MA 02118

[4]Department of Orthodontics, Boston University School of Dental Medicine, Boston, MA 02118

Abstract

Vascular formation is intimately associated with bone formation during distraction osteogenesis (DO). While prior studies on this association have focused on vascular formation locally within the regenerate, we hypothesized that this vascular formation, as well as the resulting osteogenesis, rely heavily on the response of the vascular network in surrounding muscular compartments. To test this hypothesis, the spatiotemporal sequence of vascular formation was assessed in both muscular and osseous compartments in a murine model of DO and was compared to the progression of osteogenesis. Micro-computed tomography (μCT) scans were performed sequentially, before and after demineralization, on specimens containing contrast-enhanced vascular casts. Image registration and subtraction procedures were developed to examine the co-related, spatiotemporal patterns of vascular and osseous tissue formation. Immunohistochemistry was used to assess the contributory roles of arteriogenesis (formation of large vessels) and angiogenesis (formation of small vessels) to overall vessel formation. Mean vessel thickness showed an increasing trend during the period of active distraction ($p=0.068$), whereas vessel volume showed maximal increases during the consolidation period ($p=0.009$). The volume of mineralized tissue in the regenerate increased over time ($p<0.039$), was correlated with vessel volume ($r=0.59$; $p=0.025$), and occurred primarily during consolidation. Immunohistological data suggested that: 1) the period of active distraction was characterized primarily by arteriogenesis in the surrounding muscle; 2) during consolidation, angiogenesis predominated in the intraosteal region; 3) vessel formation proceeded from the surrounding muscle into the regenerate. These data show that formation of vascular tissue occurs in both muscular and osseous compartments during

Corresponding author and address for reprint requests: Elise F. Morgan, PhD Department of Mechanical Engineering 110 Cummington Street Boston, MA 02215 e: efmorgan@bu.edu p: (617) 353-2791 f: (617) 353-5866.

DISCLOSURES

None.

DO and that periods of intense osteogenesis are concurrent with those of angiogenesis. The results further suggest the presence of morphogenetic factors that coordinate the development of vascular tissues from the intramuscular compartment into the regions of osseous regeneration.

Keywords

bone regeneration; blood vessels; muscle; micro-computed tomography; perfusion

1. INTRODUCTION

Bone formation is intimately dependent on formation of vascular tissue. Inadequate blood supply is a major cause of delayed bony union and nonunion, leading to many of the complications in various post-surgical orthopedic treatments [1, 2]. Studies of human tibial fractures have shown impaired rates of healing as high as 46% when the patient had concomitant vascular injuries [3]. Fracture healing is also greatly compromised in situations of poor muscular coverage, of loss of muscular coverage due to extensive trauma, and of associated compromise of the vascular bed [3, 4]. Surgical transfer of tissue inclusive of the surrounding muscle is commonly used to salvage extensively traumatized lower extremities, and successful outcomes are generally credited to the maintenance of undamaged vascular beds in the transferred muscle tissue [4]. In experimental studies of fracture healing, development of lower-limb ischemia, in which the surrounding vasculature is damaged, has been also shown to lead to delayed union [5]. Such findings suggest therefore that the integrity of the vascular bed within the muscular compartment is essential to bone regeneration; however, the role that the surrounding vasculature plays in the morphogenesis of the vessels in the bone is not well defined.

Vascular morphogenesis during embryological skeletogenesis occurs by collateralization of vessels from the surrounding musculature into the newly forming bones and by subsequent formation of vascular tissue via angiogenesis concurrently with formation of both cortical and trabecular bone [6–8]. However, little is known about vascular morphogenesis during post-natal skeletal regeneration after injury or surgery. A basic understanding of the mechanisms by which vascular tissue growth is patterned is essential to developing an understanding of how vascular and skeletal cells coordinate the presentation of specific morphogenetic signals to each other within developing or regenerating bone tissues. Such an understanding is also important for maximizing the success of surgical procedures for bone repair, for tissue engineering of materials that will present morphogens in a specific spatiotemporal manner, for the development of scaffolds for cell-based therapies, and for determining the optimal timing of the application of therapeutic compounds that seek to promote vascular and/or bone healing [9].

Distraction osteogenesis (DO) represents an excellent orthopedic model to study both the processes of vascularization and the functional interactions between vascular and bone formation in a post-natal context. DO is a true regenerative process in which new bone formation is stimulated by mechanical stretching of the callus that forms following resection osteotomy [10, 11]. DO is used to lengthen and reshape bones and also to correct pseudarthroses that remain refractory to other forms of treatment [12–14]. The “tension stress” that is applied to the callus, or regenerate, appears to stimulate regulatory mechanisms that inhibit cartilage formation [15, 16], and these same signals appear to also promote extensive amounts of vascularization. Previous studies from our laboratory that have examined the functional relationship between vascular morphogenesis and bone tissue morphogenesis using a murine model of DO have shown that genes associated with vascular tissue formation were induced during each round of distraction [17]. Interestingly, the extent

of vascularization has been proposed to provide many of the biological signals that direct differentiation of skeletal progenitor cells to the osteogenic lineages [18]. Consistent with this idea, we have shown that inhibition of formation of vascular tissue via antibody blockade of VEGF-receptor activity led to decreased bone formation and BMP2 expression and increased formation of cartilage and fibrous tissue [19]. Our recent findings also show that vascular smooth cells and endothelial cells are a major source of BMP2 expression during DO induced bone formation [20].

We hypothesized that the vascular network in surrounding muscular compartments would contribute to vascular formation and bone regeneration within the distraction regenerate. We tested this hypothesis by quantifying the temporal and spatial morphogenesis of vessel and bone formation across the time-course of DO in both muscular and osseous compartments. During the course of carrying out these studies, we developed and validated image-registration and image-subtraction procedures for micro-computed tomography (μCT) scans performed sequentially before and after demineralization on specimens containing contrast-enhanced vascular casts. Using these new techniques of contrast-enhanced, micro-computed tomography in conjunction with immunohistology, we specifically examined the contributory roles of arteriogenesis (formation of large vessels) and angiogenesis (formation of small vessels) to overall vascular tissue formation in both the surrounding muscular tissues and in the osseous regenerate during DO.

2. MATERIALS AND METHODS

2.1 Study Design

All animal studies were carried out under a protocol that was approved by the Institutional Animal Care and Use Committee (IACUC) at the Boston University School of Medicine. Male, C57BL/6J wild type mice were obtained from Jackson Labs (Bar Harbor, ME). All mice enrolled in the study weighed 25–35 g and were between ages 9–11 weeks of age at the time that they underwent DO surgery on the left femur. The total time-course for the experiment was 31 days. The distraction protocol consisted of three phases: 1) latency phase of seven days duration; 2) active distraction phase of ten days; and 3) a consolidation phase of 14 days. Animals were sacrificed and tissue was harvested at six post-operative days (PODs): day 7 (end of latency period), day 10 (three days into active distraction), day 14 (seven days into active distraction), day 17 (end of active distraction), day 20 (three days into consolidation), and day 31 (end of consolidation). The rate and rhythm of distraction were 0.15 mm applied once per day. The total distraction length was thus 1.5 mm at a rate of 0.15 mm per day, consistent with our previous published data [17, 19]. A total of 25 mice were used in the surgical studies with 21 going through to completion in the study. Of the four that failed to complete the study, two died during the surgery, and two did not maintain alignment during the distraction procedure. Micro-computed tomography (μCT) was carried out on 15 of the 21 animals (N=3 for POD 20; N=2 for each of PODs 7 and 14; N=4 for each of PODs 17 and 31). The remaining six mice were used for immunohistological studies (N=1 for each of PODs 7, 10, 17, and 20; N=2 for POD 31). Four additional mice (N=3 for μCT; N=1 for immunohistology) were used as un-operated controls. Euthanasia was carried out by CO_2 asphyxiation followed by cervical dislocation.

2.2 Surgical Procedure

The surgical procedure of Carvalho et al. [17] that was developed for the murine tibia was modified in this study for use in the femur. Prior to surgery, isoflurane-induced anesthesia was administered using a veterinary anesthetic machine adapted for rodents. The left hind leg of each mouse was shaved and cleaned with betadine and alcohol. An incision was made longitudinally along the parapatellar midline extending from the greater trochanter of the

femur to the patella. The femur was then elevated and carefully separated from the surrounding musculature as to avoid damaging the periosteum. A 6mm-track distraction device (KLS Martin, Jacksonville, FL) was then attached to the femur. The arms of the device were opened a distance of four mm, and the device was then secured to the bone using 0.01″ ligature wire (Dentsply International, York, PA). A low-speed, rotary, diamond disk (Benco Dental, Wilkes-Barre, PA) was then used to make a transverse osteotomy in the mid-diaphysis of the femur, centered between the arms of the distraction device. Constant saline irrigation was used to prevent any thermal necrosis. After the osteotomy procedure was completed, the proximal and distal halves of the femur were approximated. The incision was closed using 5-0, plain gut resorbable sutures (Benco Dental, Wilkes-Barre, PA). The mice were then given a 0.5mg/kg intramuscular dose of Buprenorphine to the left thigh. For the two days following surgery, the mice were given a subcutaneous 0.5mg/kg dose of Buprenorphine every 12 hours and a 0.2cc/400 g dose of Enrofloxacin every 24 hours.

2.3 Vascular Perfusion

Based on the procedure of Duvall et al. [21], the thoracic cavity was opened immediately after the animals were euthanized, and the inferior vena cava was severed. The vasculature was flushed with 0.9% normal saline containing heparin sodium (100 U/ml) via a needle inserted into the left ventricle. The specimens were then pressure-fixed with 10% neutral buffered formalin. Formalin was flushed from the vessels using heparinized saline, and the vasculature was injected with a radiopaque silicone compound containing lead chromate (Microfil MV-122, Flow Tech; Carver, MA). The intact hindlimbs were stored at 4°C overnight in 4% buffered paraformaldehyde for polymerization of the contrast agent. The fixative was changed with fresh reagent, and fixation was continued for three additional days, after which the tissues were then stored until use in neutral-buffered PBS at 4°C.

2.4 Micro-Computed Tomography (μCT) and Image Processing

In order to provide support to the regenerate after removal of the distraction device, specimens were embedded in 1% agarose made in buffered saline. Specimens were then scanned using a Scanco μCT40 system (Scanco Medical, Brüttisellen, Switzerland). Scans were carried out at a resolution of 10 μm/voxel, with voltage, current, and integration time of 70 kVp, 114 μA, and 300 ms, respectively. Specimens were then decalcified for two weeks in 14x ethylene diaminetetraacetic acid (EDTA) (Boston BioProducts, Boston, MA) at 4°C and scanned a second time using the same settings as the first scan. Decalcification was necessary to allow automated segmentation of vessel from bone tissue, because unlike in prior studies using synchrotron μCT to image vessels in unfractured bones [22], partial-volume effects resulted in overlapping intensity ranges for bone tissue and contrast agent in the images obtained prior to decalcification.

Although the perfused vasculature is readily segmented in the second (“post-decal”) scan through use of a global threshold, the decalcification process results in distortion of the tissues. Thus, the post-decal images were registered against the images from the first (“pre-decal”) scan in order to recover the original anatomic position of the vessels. The registration process used the Bookstein algorithm coded within commercial software (Amira 5.2, Visage Imaging, San Diego, CA) and involved placement of ~100 pairs of landmarks at corresponding points on the vascular network in the pre- and post-decal images. The registered, post-decal images were then subtracted from the pre-decal images in order to obtain images that were ideally devoid of vasculature and that could be used to quantify the mineralized tissue (Figure 1A). The subtraction process consisted first of binarizing the registered, post-decal images, then growing the diameter of each vessel in these images (in order to account for imperfections in the registration), and finally setting to zero the intensity of any voxel in the pre-decal images that corresponded to a location contained within a

vessel in the binarized, enlarged-vessel images. In this subtraction process, two parameters were specified: 1) the threshold that was used to binarize the registered, post-decal images; and 2) the amount that the vessels were grown (growth value). Two growth methods were evaluated (Figure 1B). In the first method, method A, each transverse cross-section of each vessel was enlarged by adding g layers of voxels around the perimeter, where g is the growth value. In method B, an isosurface was created of each vessel to provide a smoothed representation of the vessel boundary, as defined by points of equal intensity, and the isosurfaces were grown radially by g layers of voxels.

Selection of the best growth method and the best combination of threshold and growth values was carried out through a parametric analysis of two day-14 specimens and one day-17 specimen. A range of thresholds and growth values were investigated, and for each pair of values, the volume of mineralized tissue, BV, was computed by applying a global threshold (45% of the average attenuation of the cortex [23]) to the subtracted, pre-decal image. The value of BV was then added to the volume of vascular tissue, VV, which was quantified using the registered, post-decal image. This sum was compared to the volume of mineralized tissue and vessel, V_{total}, that was computed from the pre-decal image by applying the same global threshold that was used to compute BV. All volumes were computed using the analysis software of the μCT system.

Once the best combination of threshold, growth value, and growth method was identified, the subtraction process described above was carried out for each specimen. Quantitative, 3-D metrics of the vascular structure and the mineralized tissue were then obtained for two sets of volumes of interest (VOIs) in the regenerate, inclusive of the surrounding thigh musculature (Figure 1C): 1) extraosteal and intraosteal VOIs; and 2) proximal, middle, and distal VOIs. For the vascular structure, the metrics were VV, mean vessel thickness, mean vessel separation, vessel number, vessel connectivity, and vessel degree of anisotropy. These metrics were evaluated on the registered, post-decal images. For the mineralized tissue, the metrics were BV and tissue mineral density (TMD) and were evaluated on the subtracted images. A semi-automated contouring process [23] was used to exclude the pre-existing cortex from the analysis of mineralized tissue. Only VV and BV were computed for proximal, middle, and distal VOIs; the other metrics were not computed for these three additional VOIs, because each of these VOIs did not contain enough of the vascular structure to permit reliable calculation of vessel morphology.

2.5 Preparation of Tissue for Histological Analysis

Specimens used for histological analysis were recovered immediately after sacrifice. The femur was disarticulated from the acetabulum of the pelvis with the surrounding musculature kept intact, and the distraction device was left attached for added stability. The limb was cut just below the patella, keeping the knee joint intact. Harvested limbs were placed into fresh 4% paraformaldehyde for 48 hours of fixation. After this 48-hour period, the distraction device was carefully removed from the femur so as not to damage the bone and to preserve alignment across the osteotomy gap. Specimens containing the regenerate and intact muscle groups that immediately surround the bone were placed in 14% weight per volume EDTA for two weeks of decalcification. Decalcified specimens they were embedded in paraffin and sectioned in the sagittal plane. Five-micron sections were prepared making serial groups of 100 from 250 microns increments across the entire block. For standard histological assessment, sections were taken across the whole volume of tissue, and standard procedures for deparaffinization, rehydration, and staining with hemotoxylin and eosin were carried out.

2.6 Immunohistology

Sections were deparaffinized, rehydrated, and reacted with rabbit polyclonal antibodies against Von Willebrand Factor (vWF) (Millipore Inc., Medford, MA) and smooth muscle α-actin (SMA) (Sigma-Aldrich, St Louis, MO). Anti-SMA antibodies were used to detect the formation of large vessels and small arterioles and veins that contain medial layers. Anti-VWF antibodies were used to detect both the endothelial cells that line larger vessels and capillaries that are lacking medial layers. Antibody staining was carried out at the Boston University Immunohistochemistry Core facility using an automated slide stainer (IntelliPATH FLX System, BioCare Medical, Inc., Concord, CA). Antibody retrieval was carried out using Rodent Decloaker Reagent (Biocare Medical) at 90°C for 35 minutes with a cool down for ten minutes at 85°C. Background perioxidase staining was quenched by presoaking the slides in peroxidase for ten minutes. Primary antibodies for vWF and SMA were reacted at a dilution of 1:100 and 1:800 respectively at room temperature in DavinCi Green Diluent (Biocare Medical) for two hours. After the primary antibody reactions, each set of slides was washed for two minutes in TBST followed by incubation with Rabbit on Rodent HRP Polymer or Mouse on Mouse HRP Polymer (Biocare Medical) for 30 minutes. Slides were then washed in TBST for two minutes. To visualize the immune reactions, slides were incubated with DAB kit (Buffer plus diluent added on board) for five minutes. Slides were then washed with deionized water. Hematoxylin was added for one minute as a counterstain.

2.7 Statistical Analysis

Each of the μCT-derived 3-D metrics of the vascular structure and the mineralized tissue, as measured on the entire regenerate inclusive of the surrounding musculature ("total VOI", as defined in the Materials and Methods, Figure 1C), was compared across time-points (inclusive of the un-operated controls) using a Wilcoxon signed-rank test followed by Tukey *post hoc* test. Analyses of variance with repeated measures were used for the comparison of metrics in the extraosteal vs. intraosteal VOIs and in the proximal vs. middle vs. distal VOIs. Correlation analyses were carried out to identify associations between metrics of the vascular structure and metrics of the mineralized tissue for the total VOI. Regression analyses were also performed using measurements from the multiple VOIs, with the animal ID was included as a random effect in order to account for the fact that multiple data points were used from each animal (each regenerate).

3. RESULTS

3.1 Development of μCT imaging methods for the concurrent analysis of vascular and mineralized tissues

Current approaches using contrast-enhanced vascular casts and μCT to visualize vessel networks within bone organs, particularly in the context of a bone injury, do not allow clear discrimination between vessels and bone tissue at the image resolution typically afforded by desktop μCT systems. The approach that was developed in this study was to image the same specimen before and after demineralization, to co-register the two 3-D images, and then to subtract the registered second image from the first. The result is an image of the vasculature alone, with distortion induced by the demineralization process removed, as well as an image of only the mineralized tissue. Each of these images can then be subjected to quantitative, morphometric analysis. Assessment of the robustness and accuracy of this approach indicated that of the two subtraction methods evaluated, the one involving growth method B (Figure 2A right panel) yielded much smoother and smaller variations in BV for small changes in threshold and growth value (Figure 2A, left panel). For method B, combinations of high thresholds and low growth values produced values of BV+VV that were close to V_{total}; however, due to imperfections in the image registration, these combinations did not

result in removal of all of the vasculature upon image subtraction. With method B, thresholds and growth values ranging 6200–6600 and 2–3, respectively, tended to produce the most stable values of BV and resulted in a subtracted image with few residual vessels and little image noise (Figure 1B). For the best identified combination of threshold (6600), growth method (B), and growth value (3), the sum of BV and VV was on average 16.7% less than V_{total}, indicating that BV was underestimated as a consequence of needing to grow the vessels to ensure subsequently their thorough subtraction.

3.2 Time-Course of Vessel Morphogenesis During Distraction Osteogenesis

In order to assess the contributory role of external vasculature to the requisite vascular tissue formation in DO, the vasculature in the total VOI was considered. Survey of the renderings of the vasculature alone (Figure 2B, left panels) and of the composite images in which the vasculature is overlaid on the mineralized portion of the regenerate (Figure 2B, right panels) showed that very little vessel development occurred within the inner portion of the regenerate through day 17. In contrast, an immense vascular response involving development of extensive numbers of smaller vessels was seen within the intraosteal space by day 31. This set of qualitative data suggests that the majority of vascular tissue development takes place after the period of active distraction has ended, during the period of consolidation when bone tissue is being laid down [19].

The images of the vasculature in isolation were next used for quantitative analysis of vascular development during DO. The first of these analyses considered the temporal changes within intraosteal and extraosteal VOIs, as well as within the total VOI (Figure 3). Vessel volume showed a steady increase from the end of the distraction period through the end of the consolidation period such that vessel volume was greater at days 20 and 31 in comparison to day 7 ($p=0.009$). This increase over time appeared to occur initially in the extraosteal space, followed by an increase in the intraosteal space after the distraction period ended. Mean vessel thickness (luminal diameter) appeared to increase sharply at the end of the distraction period, due almost exclusively to the extraosteal contribution, and showed a strong trend towards higher values at day 17 (end of active distraction) in comparison to day 7 (end of latency) ($p=0.068$). Vessel connectivity also increased over the entire time course and was higher at day 31 compared to day 7 ($p=0.03$) and higher in the extraosteal as compared to intraosteal space. No differences among time-points were found for mean vessel number, mean vessel separation, and the degree of anisotropy of the vessels ($p>0.7$). The extraosteal space exhibited lower vessel number ($p=0.025$) and a trend towards lower degree of anisotropy ($p=0.094$). No differences in parameters were found among proximal, middle, and distal VOIs ($p>0.289$). The degree of anisotropy was greater than one for all time-points ($p<0.001$), indicating that the structure of the vessel network was preferentially oriented.

The second analysis examined the data on vessel thickness and vessel separation in more detail. The distributions of vessel thickness (Figure 3B, left panel) showed a characteristic shape across all time-points, with the majority of the vessels clustered in the thickness range of approximately 20–140 microns. From the earlier (days 7, 14, 17, 20) to the latest (day 31) time-points, the largest increase was seen in the vessels of size ranging 30–70 microns. The histograms of vessel separation (Figure 3B, middle and right panels) showed a relatively smooth and nearly symmetrical distribution over the range 0–0.8 mm. Between days 17 and 20, the peak of this portion of the distribution shifted leftward from approximately 0.57 mm to approximately 0.45 mm, indicating an overall decrease in the distance between vessels as the vascular network increased in density.

The μCT data suggested that there were two periods of vascular tissue formation: one that occurred during the active distraction period and involved enlargement of preexisting

vessels and formation of larger vessels (arteriogenesis) primarily in the extraosteal musculature; and one that occurred during the consolidation phase and involved formation of smaller vessel formation (angiogenesis), primarily in the intraosteal region. In order to probe this idea further, immunohistological analysis of the vascular tissue was examined in the context of the histological progression of bone formation. Examination of the un-operated control tissues showed the anatomical configuration of the vascular beds present in the femoral mid-diaphysis and surrounding muscle (Figure 4A). No vessel structures that reacted with SMA antibody were seen in the medullary space; however, groups of vWF-positive cells arranged in lattice-like structures were seen to comprise the vascular sinusoids in the intramedullary bone. The periosteum has very few SMA immune-reactive vessels and many flattened, VWF-positive, small vessels lining the surface of the bone. Only small vascular elements were seen in the fascia layers between muscle tissues of the control tissue, which were reactive for both SMA and vWF antibodies. Control sections incubated with non-immune rabbit serum confirmed specificity of the antibodies (Figure 4B).

Examination of tissues obtained across the time course of DO showed temporal shifts in both SMA and vWF expression (Figure 5). Three days after active distraction was initiated (POD 10), the intra-osseous space in the gap was filled with fibrous cells aligned with the axis of distraction. Many of these cells were immune positive for SMA. A very small number of small, SMA-positive vessels was also seen in this the region. In contrast to un-operated tissues, regions immediately adjacent to the periosteum and regions in the fascia between muscles contained numerous large vessels. vWF staining was seen in small, elongated vessel structures in the gap region as well as in the endothelial cells lining the larger vessels in the muscle region, but there were very few capillaries visible in the surrounding muscle tissues. By comparison, at POD 17, many fewer fibrous cells immune-positive for SMA were seen in the distraction gap, while larger vessel structures were still observed in the surrounding muscle tissues. At this time-point, as the marrow space was beginning to re-form, the vWF antibodies detected cellular structures similar to those seen in the un-operated medullary space, and large sinusoidal spaces were seen in the distraction gap. At POD 31, when the intramedullary space in the gap had filled with trabecular bone, very intense immunoreactivity was seen with both antibodies. SMA staining detected large numbers of much smaller, but well defined vessels in the surrounding muscular tissue, fascia tissues adjacent to the bone, and the intraosteal space. Small vessels surrounded with SMA-positive medial layers were even seen in the medullary space adjacent to the aligned regions of trabecular bone. Intense and numerous VWF-stained small vessels were seen both in the surrounding muscle tissues and in the intraosteal space.

3.3 Time-Course of Bone Formation during Distraction Osteogenesis and Correlations Between Vascular and Bone Formation

Quantitative analysis of the mineralized tissue was performed on the images resulting from the image registration and subtraction procedures that were developed in this study. For the total VOI and intraosteal VOI, respectively, the volume of mineralized tissue (BV) and the volume fraction of mineralized tissue (BV/TV) were higher at day 31 as compared to day 7 ($p<0.039$; Figure 6A). No temporal changes in tissue mineral density were detected (mean ± standard deviation across all time-points = 1009 ± 85 mg HA/ccm), nor were any differences found in BV and TMD among VOIs ($p>0.223$).

In order to identify associations between features of the vascular network and those of the mineralized portion of the regenerate, correlation analyses were carried out using the data from the total VOI and also using data from the multiple individual sub-volumes of the regenerate. For the total VOI, BV and vessel volume were positively correlated ($r=0.59$, $p=0.025$), and this association also held when the data from the individual VOIs were

considered (r^2 = 0.85, p=0.001). For the intraosteal VOI alone, tissue mineral density was positively correlated with vessel volume (r=0.57, p=0.016).

These correlations agreed well with histological observations of the time-course of bone and vessel formation. Although the period of active distraction was characterized primarily by large amounts of fibrous tissue aligned along the distraction axis within the gap, an asymmetric initiation of bone formation was noted in this period on the proximal ends of the gap (Figure 6B). Distraction also initiated a robust periosteal response, resulting in considerable amounts of new tissue is formed outside the original confines of the cortical bone. Three days after active distraction ceased, robust bone formation was observed bridging the gap along the periosteal surface, forming long trabecular columns of osseous tissue. The central intramedullary region remained filled with aligned, fibrous tissues; some small foci of chondroid tissues were found around both proximal and distal peripheral edges of the gap. By the end of consolidation, the gap was completely bridged with trabecular bone, and the periphery of this region was being remodeled into cortical bone. At all time-points during active distraction, well defined, larger vascular structures were seen at first within the muscular fascia located between the two layers of muscle closest to the bone (Figure 6C). As bone formation progressed during consolidation, smaller vessels were observed within the intraosteal regions in the gap center.

4. DISCUSSION

Numerous studies have shown that skeletal development and skeletal regeneration after surgery or injury are dependent on the formation of vascular tissues [5, 19, 24, 25]. Given that dysmorphic development of vascular tissues is related to a multitude of pathologies, a central focus of much of vascular tissue research is directed at the mechanisms associated with vascular morphogenesis [26, 27]. While previous studies on re-vascularization of bone injuries have focused primarily on formation of vascular tissue *within* the injury site or surgical site, we reasoned that it would be as important to examine the local vascular structure as part of the larger structural network of vessels that extends from the surrounding musculature. This examination enables insight into how changes to this network yield a vascularized regenerate and contribute to the regenerative process of DO. The results suggest that vascular morphogenesis during DO proceeds via consecutive processes of arteriogenesis in the surrounding muscular tissue and subsequent vascular in-growth into the intraosteal space through an intense period of angiogenesis both in the intraosteal space and in the region immediately peripheral to the bone. When the regenerate and surrounding musculature were considered together, vessel volume and vessel connectivity density increased between the earliest and latest time-points, while mean vessel thickness increased only during the period of active distraction. More detailed inspection of these data, via examination of the distributions of vessel thickness and vessel separation, revealed an increase in the proportion of smaller vs. larger vessels, concomitant with a decrease in a characteristic distance between vessels, between the active distraction and consolidation periods. These data describe a scenario in which formation of larger vessels and/or enlargement of existing vessels give way to a predominance of newly formed, smaller vessels once lengthening has ceased. Regional analysis of the vascular structure via μCT and immunohistology suggested that this initial phase of increased mean vessel thickness arises from enlargement and collateralization of existent larger, less closely spaced vessels in the surrounding musculature, whereas during the latter phases of DO, many smaller, more closely spaced vessels are formed in the intraosteal space.

The strengths of this study lie in the combination of newly developed image processing techniques for the μCT scans with assessments of protein expression to investigate not only the spatial and temporal correspondence between vascular tissue formation and osteogenesis

but also the morphogenesis of the vascular structure. Co-registration of the pre- and post-decal scans restored the original anatomic arrangement of the vasculature in the post-decal scans, thereby enabling regional analysis of the vessel elements and co-localization of vessels and mineralized tissue. These analyses were critical for identifying the progression of vascularization from extra- to intraosteal spaces and for elucidating associations between characteristics of the mineralized tissue (*i.e.* volume and mineral density) and vessel volume. Although the perfusion technique that we used precluded the possibility of *in vivo* assessments of blood flow, such as have been reported previously via laser Doppler imaging [28] and technetium scintigraphy [29], the μCT images provide much more detailed information on vessel size and distribution.

The immunohistology studies provided key data that corroborated the conclusions from the μCT results regarding the respective roles of arteriogenesis and angiogenesis over the time-course of DO. SMA staining clearly identified large vessels in the surrounding musculature, but not in the intraosteal space, during active distraction, and smaller vessels in both extra- and intraosteal regions by the end of consolidation. In contrast, a steady increase in small, nascent vessel structures immune positive for vWF was noted in all regions, particularly in the marrow space of the newly formed bone. These data are also notable for the immune reactions that were not clearly associated with vessel structures. Specifically, many SMA-positive, fibrous cells were observed within the distraction gap at POD 10, which is consistent with the peak in mRNA expression of Ephrin 2b (a gene associated with smooth muscle cells that would be concurrently expressed with SMA) found in the gap tissues at this time-point in our recent study on DO [20]. Prior studies have indicated that SMA expression is associated with movement of mesenchymal stem cells into the fracture callus [30] and the DO regenerate [31], and have speculated that SMA is a marker of stem cells that give rise to tissues in the fracture callus [32]. Collectively, these findings raise interesting questions about the sources of the cell populations that contribute to vascular tissue development. Whether these populations are recruited from the surrounding tissues into the regions of bone development or arise *de novo* in this space prior to osteogenesis and then assemble into vascular tissues as tissue morphogenesis progresses remains to be clarified.

This study also has several limitations. First, although significant differences in outcome parameters were found among time-points and among sub-regions of the regenerate, and significant correlations were found between characteristics of the mineralized and vascular tissues, the relatively small sample size may have prevented the observation of additional differences and correlations. Second, the process of image registration required manual input and could be subject to errors above those that would be present in fully automated processes. Imperfections in the registration results were observed, necessitating the use of a growth value greater than one and resulting in moderate underestimation of the volume of mineralized tissue. Third, despite the use of agarose gel to support the regenerate and muscle tissues once the external fixator was removed, mal-alignment of the cortices was present in some specimens, in part because of movement after removal of the fixator and in part because of some mal-alignment present post-operatively. This mal-alignment led a small amount of tissue in the extraosteal space to be classified as intraosteal, though we were careful to reduce this confounding effect by using a conservative definition of the intraosteal space. Finally, this study focused on DO and did not address whether comparable mechanisms of vascular tissue morphogenesis would be observed in other models of bone regeneration such as occurs after fracture healing. Unlike DO, fracture healing proceeds primarily via processes of endochondral bone formation, in which avascular chondrogenesis precedes primary bone formation. Thus, although previous studies have shown that inhibition of angiogenic signaling through the blockade of VEGF activity or through genetic manipulation in murine models impaired bone formation [24, 33], direct assessment of the

structural morphogenesis of vascular tissue external to the fracture callus has not been reported.

The sequence of arteriogenesis followed by angiogenesis during vascular remodeling is in agreement with a number of previous studies that have examined neovascular tissue development in models of hindlimb ischemia [34–36] and in response to vascular occlusion in vessels [37, 38]. In both scenarios, collateral arteriogenesis has been shown to occur in response to increased circumferential stress on the vascular walls or altered flow that generates increased shear stress on endothelial cells [39, 40]. Our data would suggest that the vascular tissues in the muscle responded to both the surgical injury of bone and the mechanical forces that are produced by distraction. These data would further suggest that active distraction initially produced an increase in size of the existent vessels but did not initially increase the number of new smaller vessels. This observation is consistent with prior studies that have shown that mechanical strain placed on vessels will promote smooth muscle proliferation and vascular thickening with collateral formation but will not stimulate angiogenesis [41].

Further insight into the potential role of mechanical stimuli and other cues for vasculogenesis were obtained from consideration of our regional analyses of the vasculature. The sequential peaks in expression levels of endothelial markers—first in the surrounding musculature and then in the intraosteal region—during the distraction period are indicative of a period of secondary angiogenesis within the intraosteal region. These results, in conjunction with those on the spatiotemporal morphogenesis of the vascular structure (Figures 3 and 5), would suggest that endothelial cells proliferate and migrate into this region from the extraosteal space, leading to subsequent structural morphogenesis through the period of consolidation. In light of recent data that have shown that angiogenesis is primarily driven by hypoxia [42, 43], our findings are consistent with a paradigm in which different modes of external stimuli drive different processes of vascular tissue regeneration. That is, we observe arteriogenesis occurring during the period of active distraction, when the tension is applied to the regenerate and the surrounding muscle, and we observe angiogenesis during the consolidation period, when the intraosteal tissues would be initially less vascularized and therefore be driven by a hypoxic signaling cascade.

The methods of image processing developed in this study extend the work of prior investigations that have used μCT imaging and vascular casts in bone organs to an analysis of the spatial relationships between bone and vascular tissues in an *in vivo* model of skeletal regeneration. By seeking to image both types of tissues in each specimen and to carry out regional analyses of the vasculature structure, we could not rely solely on decalcifying specimens prior to scanning, as has been done previously [19, 21, 44, 45]. At the same time, several factors prevented accurate analysis of each type of tissue using only the pre-decal scans. As compared to synchrotron μCT, which is not widely available but can image undemineralized vascular casts within bones [46, 47], desktop μCT systems offer more limited resolution and use a polychromatic beam that, as a result of beam-hardening, leads to a greater partial-volume effect. The net result of these two limitations of desktop μCT is to decrease the lower end of the intensity range that corresponds to the lead-chromate contrast agent to the point that this intensity range overlaps with that of the bone tissue. This problem could be alleviated by focusing our analyses only on the vessels of diameter several times the voxel size [48], by using a much more highly attenuating material, such as bismuth [34], for the vascular casts. However, very highly attenuating materials tend to exacerbate beam-hardening and scatter artifacts [49], which would inflate errors in estimation of bone volumes and tissue mineral densities. An additional consideration for the present study is that for bone healing, as compared to intact bones, the locations and morphologies of the regions of mineralized tissue vs. vascular cast cannot be estimated *a priori* with much

certainty. Hence, unless the two tissues can be distinguished from each other on the basis of intensity differences, the scans performed prior to decalcification are not sufficient for studying the process of vascular formation during osteogenesis. Considering all of these factors, we sought a new method of image analysis that used both pre- and post-decal scans, image registration, and image subtraction in order to allow regional analysis of both bone and vasculature, as well as co-localization of these two tissues.

In summary, the joint analysis of the formation of vascular and osseous tissues that was performed in this study indicated that these two types of tissue exhibit a close spatiotemporal correspondence with respect to both structural morphometry and temporal dynamics in molecular signaling. In particular, the period of intense angiogenesis that was concurrent with that of osteogenesis, together with the correlations between measures of vascular structure and of mineralized tissue, suggests the presence within the regenerate of shared morphogenetic factors that promote mutual development of these two tissues. In this regard, coordinating the growth and differentiation of these two tissues would appear to be structurally necessary since vessels would not be able to easily grow into the extracellular matrix of bone once the tissue becomes mineralized. In concurrent studies in which we have investigated the expression of two of the major morphogenetic signals (PlGF and BMP2) that are known to drive angiogenesis and skeletogenesis respectively, we show that smooth muscle and endothelial cells are a primary source of BMP2 expression, while mesenchymal cells are the primary source of PlGF in DO tissues, suggesting that there is a reciprocal, paracrine feedback system between the two tissues [20]. Future study of the molecular mechanisms underlying this correspondence is needed to unravel the extensive nature and mechanisms of cross-talk between cells of the endothelial and osteoblastic lineages.

Acknowledgments

Supported with grants from the National Institute of Arthritis and Musculoskeletal and Skin Diseases (PO1AR049920) TAE and LCG and AR052746, and S10 RR021072 (EFM). Institutional support was provided by the Department of Orthopaedic Surgery Boston University School of Medicine and by Boston University School of Medicine.

References

1. Carano RA, Filvaroff EH. Angiogenesis and bone repair. Drug Discov Today. 2003; 8:980–9. [PubMed: 14643161]
2. Einhorn TA, Laurencin CT, Lyons K. Fracture repair: challenges, opportunities, and directions for future research. AAOS-NIH symposium: Bone Joint Surg Am. 2008:438–42.
3. Dickson KF, Katzman S, Paiement G. The importance of the blood supply in the healing of tibial fractures. Contemp Orthop. 1995; 30:489–93. [PubMed: 10150380]
4. Park S, Han SH, Lee TJ. Algorithm for recipient vessels selection in free transfer to the lower extremity. Plast Reconstr Surg. 1999; 103:1937–48. [PubMed: 10359256]
5. Lu C, Miclau T, Hu D, Marcucio R. Ischemia leads to delayed union during fracture healing: a mouse model. J Orthop Res. 2007; 25:51–61. [PubMed: 17019699]
6. Seichert V, Rychter Z. Vascularization of developing anterior lamb of the chick embryo. II. Differentiation of vascular bed and its significance for the location of morphogenetic processes inside the limb bud. Folia Morphol (Praha). 1972; 20:352–361. [PubMed: 4637579]
7. Seichert V, Rychter Z. Vascularization of the developing anterior limb of the chick embryo. 3. Developmental changes in the perimetacarpal capillary network. Folia Morphol (Praha). 1972; 20:397–405. [PubMed: 4637581]
8. Eshkar-Oren I, Viukov SV, Salameh S, Krief S, Oh CD, Akiyama H, Gerber HP, Ferrara N, Zelzer E. The forming limb skeleton serves as a signaling center for limb vasculature patterning via regulation of Vegf. Development. 2009; 136:1263–72. [PubMed: 19261698]

9. Fröhlich M, Grayson WL, Wan LQ, Marolt D, Drobnic M, Vunjak-Novakovic G. Tissue engineered bone grafts: biological requirements, tissue culture and clinical relevance. Curr Stem Cell Res Ther. 2008; 3:254–64. [PubMed: 19075755]
10. Meyer U, Meyer T, Wiesman HP, Kruse-Losler B, Vollmer D, Stratmann U, Joos U. Mechanical tension in distraction osteogenesis regulates chondrocytic differentiation. Int J Oral Maxillofac Surg. 2001; 30:522–530. [PubMed: 11829235]
11. Lewinson D, Maor G, Rozen N, Rabinovich I, Stahl S, Rachmiel A. Expression of vascular antigens by bone cells during bone regeneration in a membranous bone distraction system. Histochem Cell Biol. 2001; 116:381–8. [PubMed: 11735002]
12. Ilizarov GA. Clinical application of the tension-stress effect for limb lengthening. Clin Orthop. 1990:8–26. [PubMed: 2403497]
13. Dendrinos GK, Katsioulas K, Krallis PN, Lyritsis E, Papagiannopoulos G. Treatment of femoral and tibial septic pseudarthrosis by internal lengthening. Rev Chir Orthop Reparatrice Appar Mot. 1995; 80:44–50. [PubMed: 7863037]
14. Paley D, Catagni MA, Argnani F, Villa A, Benedetti GB, Cattaneo R. Ilizarov treatment of tibial nonunions with bone loss. Clin Orthop. 1989; 241:146–65. [PubMed: 2924458]
15. Jazrawi LM, Majeska RJ, Klein ML, Kagel E, Stromberg L, Einhorn TA. Bone and cartilage formation in an experimental model of distraction osteogenesis. J Orthop Trauma. 1998; 12:111–6. [PubMed: 9503300]
16. Sato M, Ochi T, Nakase T, Hirota S, Kitamura Y, Nomura S, Yasui N. Mechanical tension-stress induces expression of bone morphogenetic protein (BMP)-2 and BMP-4, but not BMP-6, BMP-7, and GDF-5 mRNA, during distraction osteogenesis. J Bone Miner Res. 1999; 14:1084–95. [PubMed: 10404008]
17. Carvalho RS, Einhorn TA, Lehmann W, Edgar C, Al-Yamani A, Apazidis A, Pacicca D, Clemens TL, Gerstenfeld LC. The role of angiogenesis in a murine tibial model of distraction osteogenesis. Bone. 2004; 34:849–61. [PubMed: 15121017]
18. Hilton MJ, Tu X, Cook J, Hu H, Long F. Ihh controls cartilage development by antagonizing Gli3, but requires additional effectors to regulate osteoblast and vascular development. Development. 2005; 132:4339–51. [PubMed: 16141219]
19. Jacobsen KA, Al-Aql ZS, Wan C, Fitch JL, Stapleton SN, Mason ZD, Cole RM, Gilbert SR, Clemens TL, Morgan EF, Einhorn TA, Gerstenfeld LC. Bone formation during distraction osteogenesis is dependent on both VEGFR1 and VEGFR2 signaling. J Bone Miner Res. 2008; 23:596–609. [PubMed: 18433297]
20. Matsubara H, Hogan DE, Morgan EF, Mortolock DP, Einhorn TA, Gerstenfeld LC. Vascular tissues are a primary source of BMP2 expression during bone formation induced by distraction osteogenesis. Bone. 2012
21. Duvall CL, Taylor WR, Weiss D, Wojtowicz AM, Guldberg RE. Impaired angiogenesis, early callus formation, and late stage remodeling in fracture healing of osteopontin-deficient mice. J Bone Miner Res. 2007; 22:286–97. [PubMed: 17087627]
22. Schneider PKT, Meyer E, Ulmann-Schuler A, Weber B, Stampanoni M, Müller R. Simultaneous 3D visualization and quantification of murine bone and bone vasculature using micro-computed tomography and vascular replica. Microsc Res Tech. 2009; 72:690–701. [PubMed: 19360841]
23. Morgan EF, Mason ZD, Chien KB, Pfeiffer AJ, Barnes GL, Einhorn TA, Gerstenfeld LC. Micro-Computed Tomography Assessment of Fracture Healing: Relationships among Callus Structure, Composition, and Mechanical Function. Bone. 2009; 44:335–44. [PubMed: 19013264]
24. Street J, Bao M, deGuzman L, Bunting S, Peale FV Jr, Ferrara N, Steinmetz H, Hoeffel J, Cleland JL, Daugherty A, van Bruggen N, Redmond HP, Carano RA, Filvaroff EH. Vascular endothelial growth factor stimulates bone repair by promoting angiogenesis and bone turnover. Proc Natl Acad Sci U S A. 2002; 99:9656–61. [PubMed: 12118119]
25. Peng H, Usas A, Olshanski A, Ho AM, Gearhart B, Cooper GM, Huard J. VEGF improves, whereas sFlt-1 inhibits, BMP2-induced bone formation and bone healing through modulation of angiogenesis. J Bone Miner Res. 2005; 20:2017–2027. [PubMed: 16234975]
26. Jain RK. Molecular regulation of vessel maturation. Nat Med. 2003; 9:685–93. [PubMed: 12778167]

27. Semenza GL. Vasculogenesis, angiogenesis, and arteriogenesis: mechanisms of blood vessel formation and remodeling. J Cell Biochem. 2007; 102:840–7. [PubMed: 17891779]
28. Zheng LW, Ma L, Cheung LK. Changes in blood perfusion and bone healing induced by nicotine during distraction osteogenesis. Bone. 2008; 43:355–61. [PubMed: 18538646]
29. Aronson J. Temporal and spatial increases in blood flow during distraction osteogenesis. Clin Orthop. 1994:124–31. [PubMed: 8156663]
30. Kinner B, Gerstenfeld LC, Einhorn TA, Spector M. Expression of smooth muscle actin in connective tissue cells participating in fracture healing in a murine model. Bone. 2002; 30:738–45. [PubMed: 11996913]
31. Kinner B, Pacicca DM, Gerstenfeld LC, Lee CA, Einhorn TA, Spector M. Expression of smooth muscle actin in cells involved in distraction osteogenesis in a rat model. J Orthop Res. 2003; 21:20–7. [PubMed: 12507576]
32. Grcevic D, Pejda S, Matthews BG, Repic D, Wang L, Li H, Kronenberg MS, Jiang X, Maye P, Adams DJ, Rowe DW, Aguila HL, Kalajzic I. In vivo fate mapping identifies mesenchymal progenitor cells. Stem Cells. 2012; 30:187–96. [PubMed: 22083974]
33. Zelzer E, Mamluk R, Ferrara N, Johnson RS, Schipani E, Olsen BR. VEGFA is necessary for chondrocyte survival during bone development. Development. 2004; 131:2161–71. [PubMed: 15073147]
34. Li W, Shen W, Gill R, Corbly A, Jones B, Belagaje R, Zhang Y, Tang S, Chen Y, Zhai Y, Wang G, Wagle A, Hui K, Westmore M, Hanson J, Chen YF, Simons M, Singh J. High-resolution quantitative computed tomography demostrating selective enhancement of medium-size collaterals by placental growth factor-1 in the mouse ischemic hindlimb. Circulation. 2006; 113:2445–53. [PubMed: 16702473]
35. Deindl E, Schaper W. The art of arteriogenesis. Cell Biochem Biophys. 2005; 43:1–1. [PubMed: 16043879]
36. Oses P, Renault MA, Chauvel R, Leroux L, Allières C, Séguy B, Lamazière JM, Dufourcq P, Couffinhal T, Dupláa C. Mapping 3-dimensional neovessel organization steps using micro-computed tomography in a murine model of hindlimb ischemia-brief report. Arterioscler Thromb Vasc Biol. 2009; 29:2090–2. [PubMed: 19745199]
37. Jacoby C, Böring YC, Beck A, Zernecke A, Aurich V, Weber C, Schrader J, Flögel U. Dynamic changes in murine vessel geometry assessed by high-resolution magnetic resonance angiography: a 9. 4T study. J Magn Reson Imaging. 2008; 28:637–45. [PubMed: 18777558]
38. van Weel V, de Vries M, Voshol PJ, Verloop RE, Eilers PH, van Hinsbergh VW, van Brockel JH, Quax PH. Hypercholesterolemia reduces collateral artery growth more dominatnly than hyperglycemia or insulin resistance in mice. Arterioscler Thromb Vasc Biol. 2006; 26:1383–90. [PubMed: 16574899]
39. Eitenmüller I, Volger O, Kluge A, Troidl K, Barancik M, Cai WJ, Heil M, Pipp F, Fischer S, Horrevoets AJ, Schmitz-Rixen T, Schaper W. The range of adaptation by collateral vessels after femoral artery occlusion. Circ Res. 2006; 99:656–62. [PubMed: 16931799]
40. Sager HB, Middendorff R, Rauche K, Weil J, Lieb W, Schunkert H, Ito WD. Temporal patterns of blood flow and nitric oxide synthase expression affect macrophage accumulation and proliferation during collateral growth. J Angiogenes Res. 2010; 16:18. [PubMed: 20843382]
41. Hershey JC, Baskin EP, Glass JD, Hartman HA, Gilberto DB, Rogers IT, Cook JJ. Revascularization in the rabbit hindlimb: dissociation between capillary sprouting and arteriogenesis. Cardiovasc Res. 2001; 49:618–625. [PubMed: 11166275]
42. Cassavaugh J, Lounsbury KM. Hypoxia-mediated biological control. J Cell Biochem. 2011; 112:735–44. [PubMed: 21328446]
43. Schipani E, Maes C, Carmeliet G, Semenza GL. Regulation of osteogenesis-angiogenesis coupling by HIFs and VEGF. J Bone Miner Res. 2009; 24:1347–53. [PubMed: 19558314]
44. Shen X, Wan C, Ramaswamy G, Mavalli M, Wang Y, Duvall CL, Deng LF, Guldberg RE, Eberhart A, Clemens TL, Gilbert SR. Prolyl hydroxylase inhibitors increase neoangiogenesis and callus formation following femur fracture in mice. J Orthop Res. 2009; 27:1298–305. [PubMed: 19338032]

45. Moore DC, Leblanc CW, Muller R, Crisco JJ 3rd, Ehrlich MG. Physiologic weight-bearing increases new vessel formation during distraction osteogenesis: a micro-tomographic imaging study. J Orthop Res. 2003; 21:489–96. [PubMed: 12706022]

46. Schneider P, Krucker T, Meyer E, Ulmann-Schuler A, Weber B, Stampanoni M, Müller R. Simultaneous 3D visualization and quantification of murine bone and bone vasculature using micro-computed tomography and vascular replica. Microsc Res Tech. 2009; 72:690–701. [PubMed: 19360841]

47. Fei J, Peyrin F, Malaval L, Vico L, Lafage-Proust MH. Imaging and quantitative assessment of long bone and vasculature. Microsc Res Tech. 2010; 293:215–24.

48. Sider KL, Song J, Davies JE. A new bone vascular perfusion compound for the simultaneous analysis of bone and vasculature. Microsc Res Tech. 2010; 73:665–72. [PubMed: 19941297]

49. Kak, AC.; Slaney, M. Principles of Computerized Tomographic Imaging. New York: IEEE Press; 1988.

Highlights

- We examined the contribution of the vascular network in surrounding muscle compartments to distraction osteogenesis.
- The period of active distraction was characterized by arteriogenesis in the surrounding muscle.
- During consolidation, angiogenesis predominated in the intraosteal region.
- Vessel formation proceeded from the surrounding muscle into the regenerate.

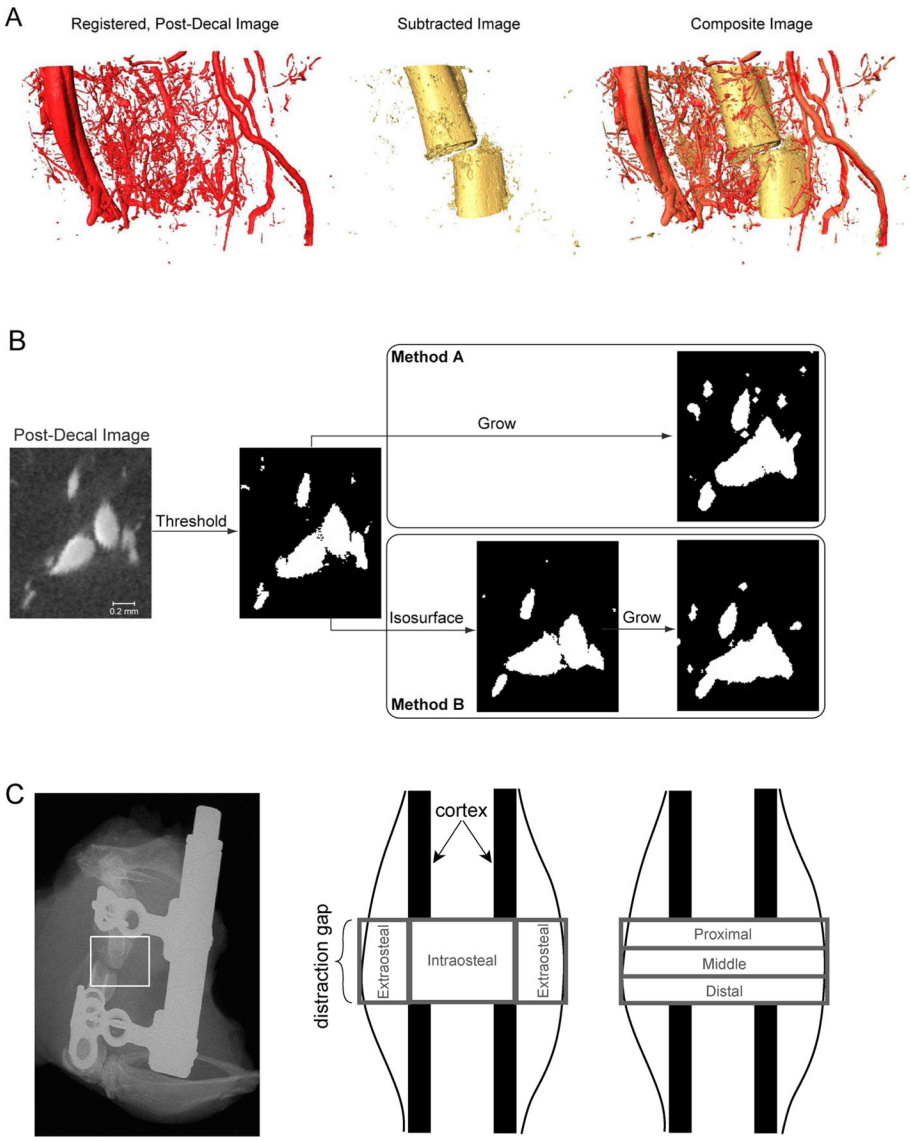

Figure 1. Methods for using μCT to co-localize and to analyze vascular and mineralized tissues within the distraction regenerate and the surrounding musculature

(A) Shown at the left is a rendering of the vasculature (POD 14) after image registration was carried out on the post-decalcification image in order to remove distortion of the tissues that occurs when the mineral is removed. Subtraction of this registered image from the pre-decalcification image produces an image of the mineralized tissue alone (shown in the middle). Examination of the composite image of bone and vasculature (shown on the right), obtained from overlaying the subtracted image on the pre-decalcification image, allows analysis of the spatial relationship between vascular and osseous tissues. Even though plain-film, radiographic assessments will show optimal alignment before the device is removed, some slippage and misalignment can occur when the bone is embedded in agarose, as seen with the reconstructed images. **(B)** As represented on a small region of a 2-D cross-section of one image, the process of image subtraction involved first binarizing the registered post-decal image in order to segment the vasculature and then growing the vessels by a small amount prior to subtracting the image from the pre-decal image. The two growth methods that were evaluated are illustrated for a growth value of 3. For the second method (method

B), the isosurface representation of the vessels is shown in the intermediate step to illustrate how the isosurface is smoother than the original vessel boundaries determined purely by thresholding; growth is applied to the isosurface rather than the original boundaries. **(C)** Two types of regional analysis were carried out on the portion of the regenerate, inclusive of surrounding musculature, located between the two osteotomy cuts. In the first, the regenerate was partitioned into intraosteal and extraosteal volumes of interest (VOIs), and in the second the partitioning was into proximal, middle, and distal VOIs. The union of each of these two sets of VOIs was dubbed the “total VOI”.

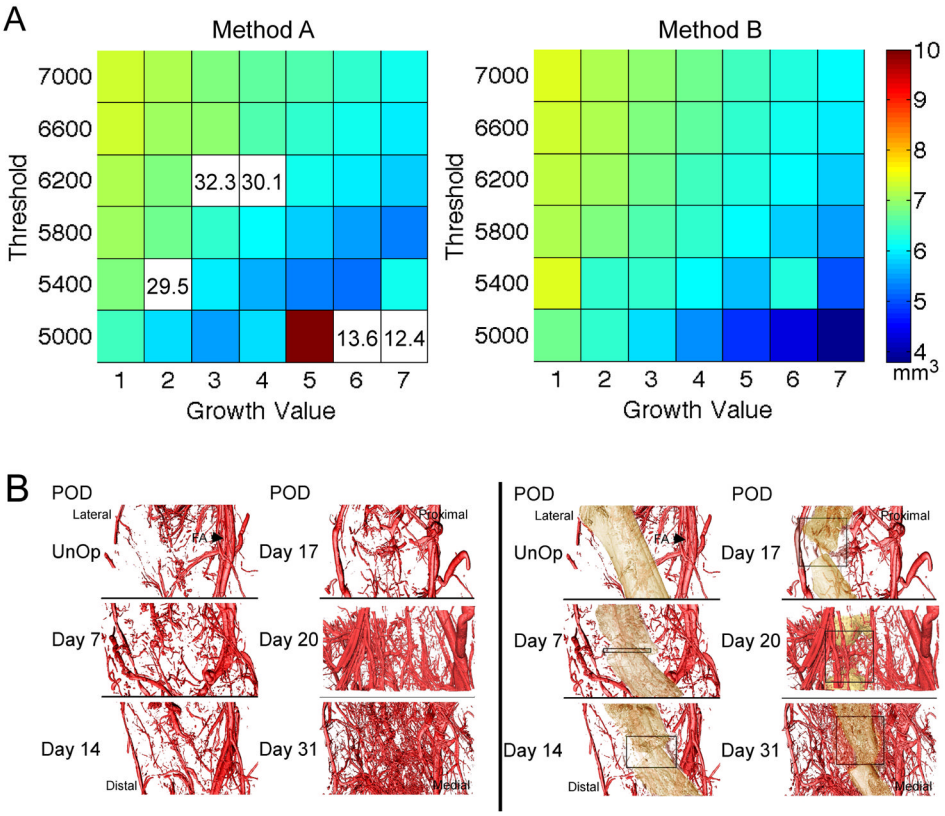

Figure 2. Results of the μCT methods to co-register vasculature and bone tissues

(A) The volume of mineralized tissue (BV (mm^3)) is shown on the colorplots as a function of threshold (16-bit scale) and growth value for the two growth methods. For growth method A, some combinations of threshold and growth value yielded extreme values of BV; these values are outside the color range and are instead listed on the plot. **(B)** Representative renderings of the vasculature (left side) and the vasculature and mineralized tissue (right side) across the time-course of DO. Vascular tissues are false-colored red. Mineralized tissue is false-colored tan. The position of the femoral artery (FA) is denoted with an arrow in the renderings of the un-operated controls. Boxes are approximations of the total width of the distraction gap at each time-point.

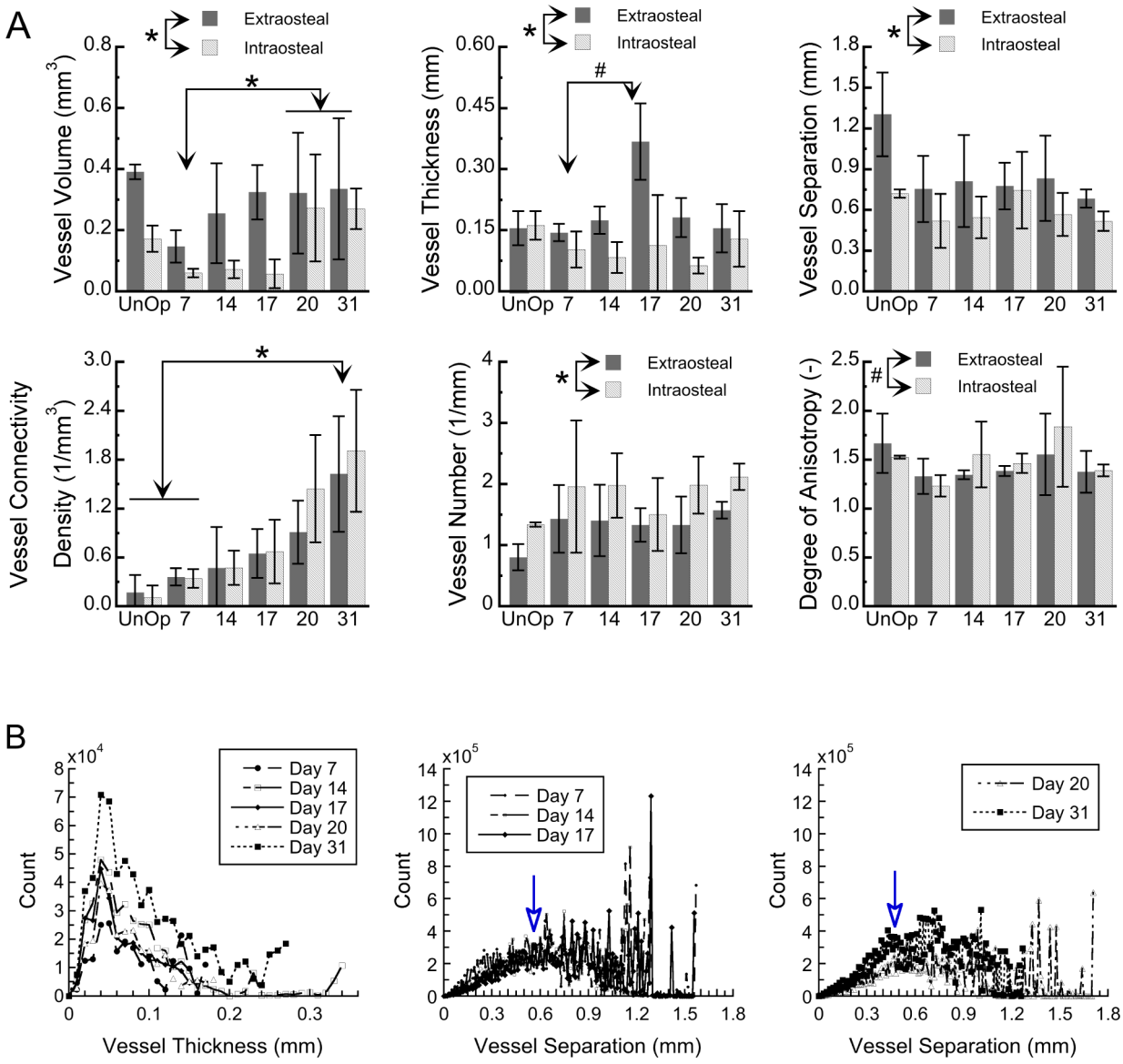

Figure 3. Morphometric analysis of the 3-D vascular reconstructions over the 31-day time-course of distraction osteogenesis

(A) Vessel volume and morphometric parameters of the vessel network are shown for the extraosteal and intraosteal VOIs at each time-point and for un-operated controls ("UnOp"). Post-operative day is indicated on the abcissa. Column heights and error bars indicate group means and standard deviations, respectively. *: $p<0.05$. #: $0.05<p<0.10$. **(B)** Histograms showing the entire distributions of vessel thickness (left panel) and vessel separation (middle and right panels) throughout the regenerate and surrounding musculature, averaged over all specimens at a given time-point. Arrows indicate the peaks in the symmetric portions of the distributions of vessel separation. Note the leftward shift in the position of the arrow from day 17 to day 20, indicating a decrease from the earlier to later timepoints in a characteristic separation distance between vessels.

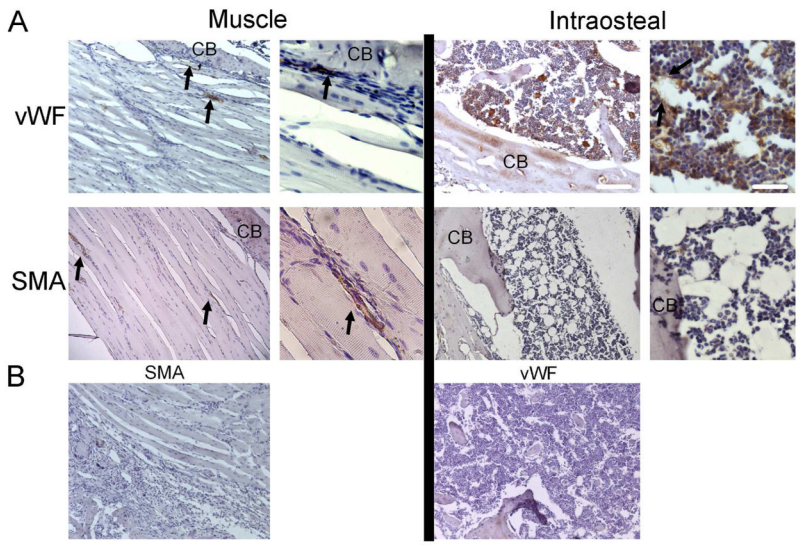

Figure 4. Identification of Vascular Structures in Un-Operated Control Tissues

(A) Selected micrographs (100x and 400x) of immunohistological analysis of smooth muscle actin (SMA; associated with arteriogenesis) and von Willibrand factor (vWF; associated with angiogenesis) in muscle and bone tissue from the femoral mid-diaphyseal region are shown. Arrows indicate immune positive structures, and 'CB' indicates cortical bone. White scale bars are of length 200 and 50 microns, respectively, for the low- and high-magnification images. **(B)** Micrographs (100x) of control sections incubated with species-appropriate, non-immune serum and secondary antibody conjugates

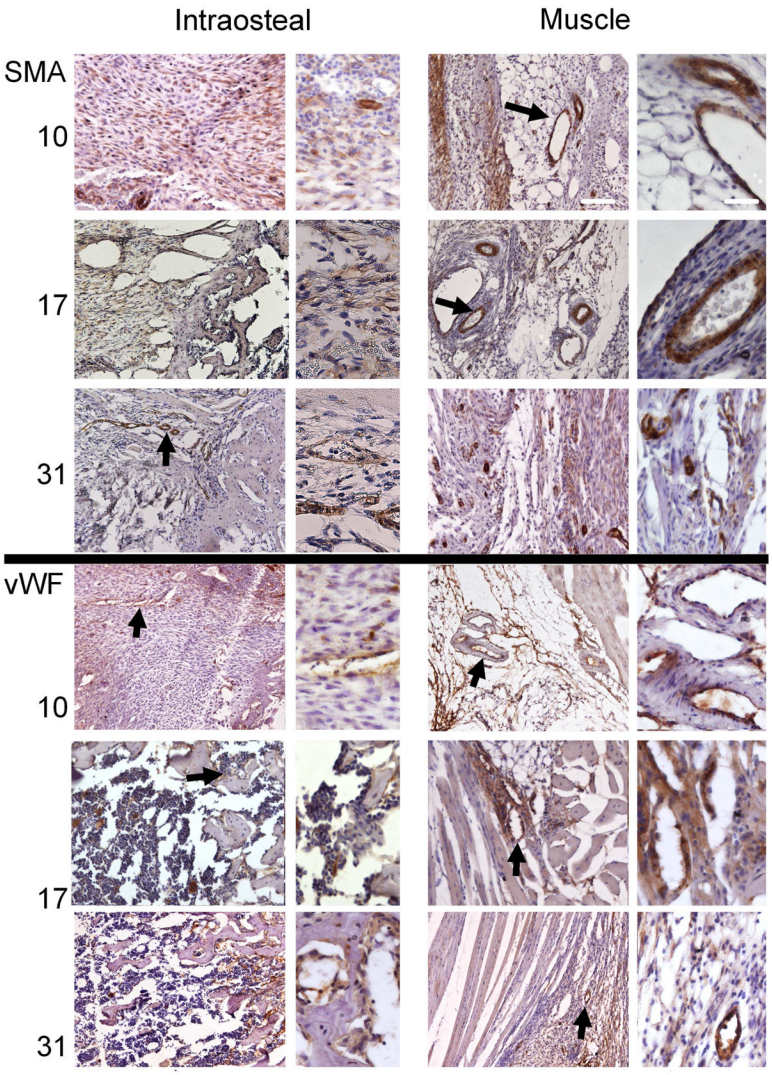

Figure 5. Immunohistological assessments of vessel formation during distraction osteogenesis

Selected micrographs (100x and 400x) of immunohistological analysis of smooth muscle actin (SMA; associated with arteriogenesis) and von Willibrand factor (vWF; associated with angiogenesis) were taken from muscular areas surrounding the distraction gap and from the intraosteal region, as defined by the periosteal margin, at days 10, 17, and 31. Time-points are listed in the left margin. Bold arrows indicate immune-positive structures that are shown in greater detail in the adjacent higher-magnification images. The micrographs showing intraosteal regions are always oriented so that the long axis of the bone is displayed horizontally, with the proximal direction at the left. The micrographs showing muscle tissues are oriented so that the diaphysis, which is vertically oriented, is to the right of the field of view. White scale bars are of length 200 and 50 microns, respectively, for the low- and high-magnification images.

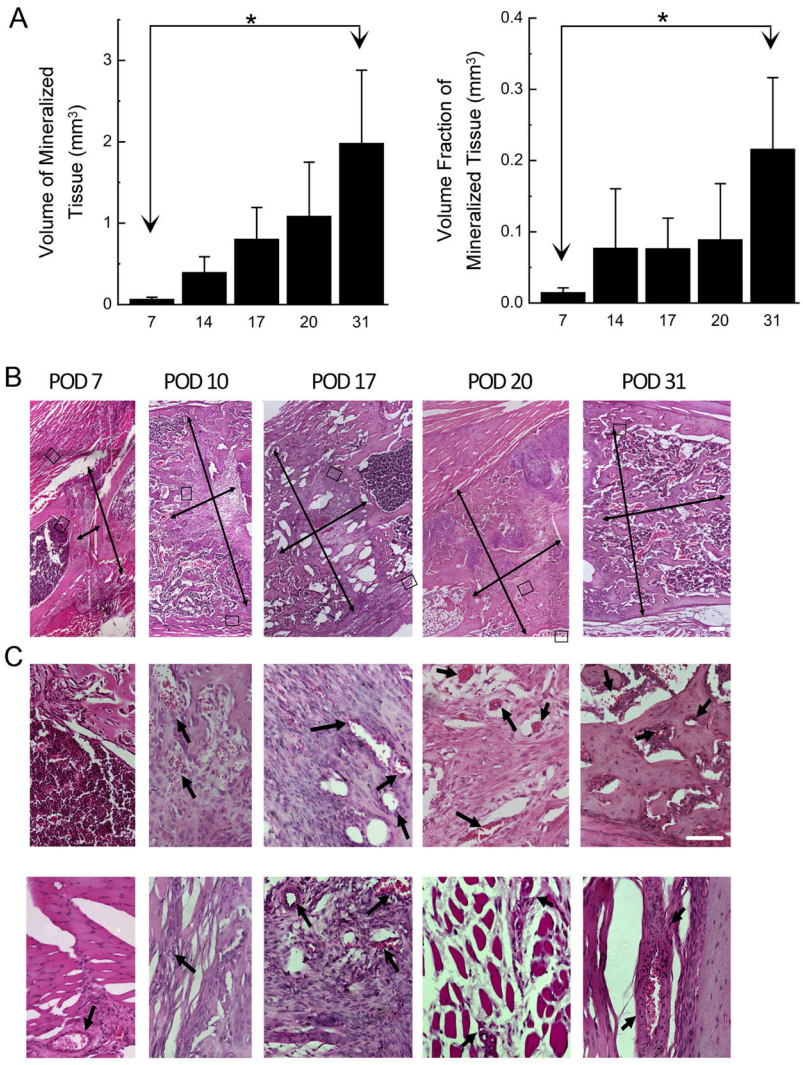

Figure 6. Analysis of the mineralized tissue and associations between vascular and osseous tissues

(A) Volume of mineralized tissue in the total VOI (left graph) and volume fraction of mineralized tissue in the intraosteal VOI (right graph) for each time-point (postoperative day is indicated on the abcissa). Column heights and error bars indicate group means and standard deviations, respectively. *: $p<0.05$. **(B)** Representative histological progression of tissue development over the time-course of DO. Images are composites made from a montage of 100x micrographs taken in the mid-diaphyseal region. Thin arrows indicate the length and width of the gap region, inclusive of the robust periosteal response. Images are oriented so that the long axis of the bone is displayed approximately left to right in a proximal to distal manner. White scale bar represents 400 microns. **(C)** Higher-magnification (400x) micrographs of the intraosteal regions (top row) and muscular regions (bottom row) boxed in (B) show specific details to highlight aspects of vessel formation in the gap during active distraction and in the surrounding muscle at other time points. The region of muscle shown for POD 31 is out of the corresponding field of view shown in (B). Arrows denote specific vessel structures. White scale bar represents 100 microns.